ELSEVIER

Journal of Alloys and Compounds 216 (1994) 187–195

Journal of ALLOYS AND COMPOUNDS

The temperature-dependent changes of the kinetics and morphology of hydride formation in zirconium

Joseph Bloch

Nuclear Research Center-Negev, PO Box 9001, Beer-Sheva, Israel

Received 18 March 1994

Abstract

The hydriding kinetics and hydride phase development in vacuum-annealed Zr were studied at temperatures ranging from 250 to 800 °C, under H_2 at 1 atm. In the lower temperature range a hydride external layer is formed with a well-defined metal–hydride interface. Between 350 and 550 °C the hydriding reaction consists of two stages: initial fast penetration of hydrogen through grain boundaries, and subsequent development of hydride layer resulting in a decrease in the advancing front velocity. The activation energy for both processes is similar (67 kJ mol^{-1}) although the front velocity of the grain boundaries is somewhat faster. Above 550 °C, where the β phase is formed in front of the δ phase, a significant change is observed in the hydriding kinetics and topochemistry. No external reaction front is formed and the hydriding route of the grain boundaries exclusively prevails with simultaneous decrease in the overall reaction rate. The activation energy for the hydride layer advance at this range, due to the diffusion of hydrogen in the β-zirconium product, or the $\alpha \rightarrow \beta$ phase transformation, is 165 kJ mol^{-1}. The huge discrepancies between the results of high temperature hydrogen diffusion in zirconium hydrides previously published are accounted for in terms of the hydriding topochemical mechanism.

Keywords: Kinetics; Hydride formation; Zirconium; Temperature dependence

1. Introduction

In recent work [1], we have shown that the hydriding reaction of bulk vacuum-annealed zirconium metal at 400 °C and under H_2 at 1 atm follows double-stage kinetics. In the initial fast stage, hydrogen preferentially penetrates into the metal through grain boundaries, resulting in hydride phase formation along these boundaries. This fast initial stage has been correlated to the preferential high temperature, low pressure oxidation observed along grain boundaries during pre-annealing. The hydride grows into the grains until the sample is entirely covered with an external hydride product layer. For sufficiently thick samples (i.e. samples for which the smallest dimension is large compared with the average grain size) the succeeding main stage is associated with the advance of this external product layer into the bulk metal according to contracting-envelope kinetics, without any further grain boundary preference. Such a hydride layer was metallographically observed on partially hydrided Zr samples at about 400 °C [1] and 300 °C [2]. A rate-controlling step of hydrogen diffusion through a δ- or ϵ-hydride product layer of constant thickness has been suggested for the system at this main stage, in agreement with previously published data [1].

It is expected that the above mechanism will change when the reaction temperature exceeds 546 °C, the eutectoid temperature [3]. The formation of the hydrogen-induced β phase above this temperature markedly modifies the properties of the product hydride layer. Above the eutectoid temperature, much more hydrogen can be absorbed (33 at.% H) prior to the $\beta \rightarrow \delta$ transformation, compared with the relatively small amount of hydrogen (6.1 at.% H) required for the $\alpha \rightarrow \delta$ transformation below the eutectoid temperature. This leads to the conclusion that a substantial portion of the steady state advancing hydride layer consists of β phase. As a result, the steady state thickness of the δ and ϵ phases may change considerably, thus inducing changes in the steady state diffusion rate. Of course, the mechanism may become entirely different owing to the presence of the new phase, with another rate-limiting step dominating the reaction rate.

SSDI 0925-8388(94)01270-R

It is interesting that almost no hydrogen absorption experiments were performed for Zr above 550 °C [4]. A deviation from the straight line of the Arrhenius plot was observed at 500 °C [5]. This was attributed to an exothermic heating effect. Hydrogen absorption in zirconium samples shaped in the forms of cylinders and spheres was measured by Gelezunas et al. [6] at high temperatures, above the eutectoid temperature. They have assumed that the rate-limiting step is diffusion through the β phase and obtained diffusion coefficients for hydrogen. There was a very large and significant difference between their results and those obtained by Albrecht and Goode [7] who measured the diffusion using the permeation technique. The attempted explanation for this difference, which is due to the presence of oxide layers affecting the absorption rate, is not satisfactory, since at these elevated temperatures the oxide layer tends to dissolve into the bulk zirconium under non-oxidizing (high vacuum) conditions [8]. The phenomenon of oxide dissolution into the bulk metal under high vacuum conditions is not unique to zirconium. It was found also for other metals such as uranium [9].

In the present work the kinetics of the zirconium hydriding reaction were studied in the temperature range 250–800 °C and under H_2 at 1 atm with the purpose of observing any temperature-dependent changes which could be related to the different phases likely to be formed during the reaction. The hydriding kinetic curves of samples with well-defined geometry (usually in the shape of a rectangular parallelepiped) were measured and correlated with the topochemistry of hydride development in partially hydrided samples. Measurements of the time dependence of the pressure drop due to the reaction were performed in a quartz constant-volume Sieverts system. The kinetic results are presented in the form of curves of $\alpha(t)$, the hydriding reaction fraction, vs. t, the time. $\alpha(t)$ is obtained from the ratio $\Delta p(t)/\Delta p_{max}$, where $\Delta p(t)$ is the pressure drop caused by the hydrogen absorption at time t and Δp_{max} is the maximum pressure drop after equilibrium conditions were achieved. More detailed descriptions of the experimental apparatus, the sample composition and preparation procedures have been published elsewhere [1].

2. Metallographic examination of partially hydrided samples

The hydride phase development in bulk zirconium as a function of temperature was studied by examining metallographic cross-sections of partially hydrided samples. The significant changes in the hydriding topochemistry at three representative temperatures are shown in Fig. 1. At low temperatures (Fig. 1(a)) a distinctive and relatively uniform hydride layer is formed on the surface of the sample. At about 400 °C, a similar layer is formed, although it is much less uniform. Some grain boundary penetration can be observed. As discussed above in Section 1, the situation shown in Fig. 1(b) is characteristic of the main stage, in which the sample is entirely covered with an external hydride layer. The intergranular penetrations observed in front of the layer are just the remaining part of the initial stage, during which the two competing processes (i.e. grain boundary penetration and layer formation) were playing a comparable role. In the high temperature sample (Fig. 1(c)), however, the significance of the grain boundary penetration is increased. No layer formation can be observed and the hydrogen seems to diffuse freely through the grain boundaries. A very low extent of reaction (i.e. $\alpha = 0.0083$) was required for this case. At higher reaction fractions (i.e. larger α), it was difficult to distinguish between the hydride and metal phases and to identify the origin of hydride phase development at the grain boundaries. Note the higher hydride concentration at the sample's corner (upper left part of Fig. 1(c)). This structure is indicative of diffusion-controlled advance of hydrogen dissolving into the sample at this high temperature. For experiments in which α is larger than 10%, this structure is observed throughout most of the bulk of the sample.

A better look (higher magnification) at the temperature dependence of the structure of the hydride–metal interfaces is given in Fig. 2. At 250 °C the interface is rather sharp and uniform, with columnar structure of the interfacial hydride. A crack passing in parallel to the interface at a distance of around 20 μm can be observed. However, one cannot tell whether this crack was actually formed during the reaction or later, following the system evacuation and cooling of the sample. At 400 °C, the interface is not as well defined as that in 250 °C. Needle-like penetrations along preferred crystallographic orientations are observed (Fig. 2(b)). They are probably the result of hydrogen dissolved in the metal at the metal–hydride interface during the reaction, precipitating when the sample is cooled to room temperature. The solubility of hydrogen in α-Zr at 400 °C is around 2 at.% [10], while at room temperature the solubility is reduced by more than three orders of magnitude. Similar lamellar hydrides originating in dissolved hydrogen were identified in partially hydrided rare earth samples [11]. The metal–hydride interface formed intergranularly at 630 °C (Fig. 2(c)) is poorly defined. It appears in the form of patches with a low degree of orientation. The large difference between the hydride phase structures observed at low and high temperatures is associated with the β phase formed during the higher temperature hydriding. When

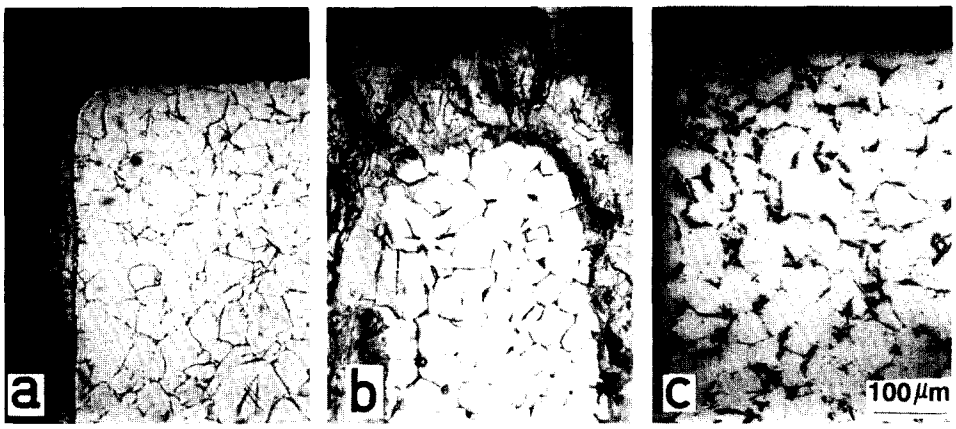

Fig. 1. Cross-section metallography of partially hydrided zirconium samples. The hydrogen pressure was 1 atm. The reaction temperatures and the reaction fractions α respectively are as follows: (a) 250 °C, $\alpha=0.1$; (b) 400 °C, $\alpha=0.25$; (c) 630 °C, $\alpha=0.0083$.

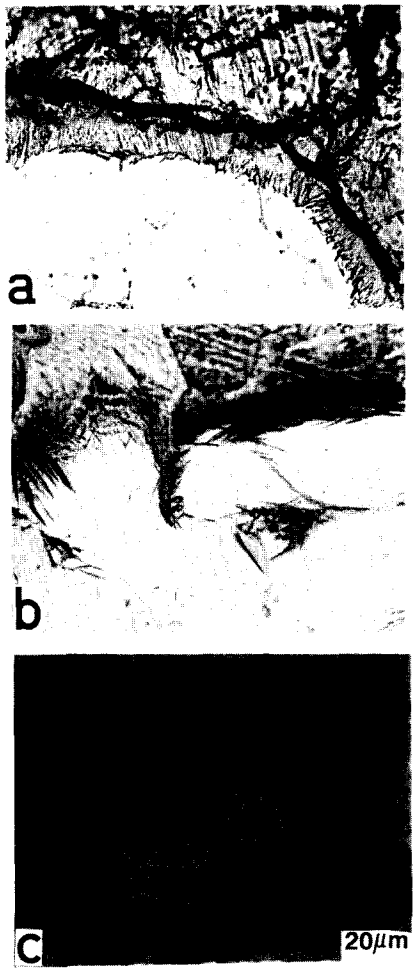

Fig. 2. Metallography of the hydride–metal interface in zirconium at different reaction temperatures: (a) 250 °C, (b) 400 °C; (c) 630 °C.

the sample is cooled, this phase transforms into the δ- and ϵ-hydrides. The rate of these transformations is very fast (in contrast with the reverse process [12]). This accounts for the relatively finely dispersed metal and hydride phases constructing the sample, as shown in Fig. 2(c).

Several successive stages of the penetration of hydrogen into the metal and the development of the hydride phases in zirconium at 630 °C are shown in Fig. 3. After annealing a reference sample at 900 °C for 2 h, it was cooled slowly to 630 °C and then brought to room temperature by removing the furnace. This procedure simulates the heat cycle experienced by the reacted samples. The micrograph of this sample is shown in Fig. 3(a). Note the small amounts of intergranular oxide resulting from the high temperature vacuum annealing [1]. The advance of the hydride phase from the grain boundaries inwards is shown in Figs. 3(b) and 3(c), taken from different areas of the same partially hydrided sample. Owing to diffusion, the extent of hydride progression formed at the surface vicinity (Fig. 3(c)) is higher than that in the sample's deeper areas (Fig. 3(b)). As mentioned above, when the reaction fraction exceeds some 10%, the whole sample seems to be homogeneously transformed. This is shown in Fig. 3(d) for a 30% hydrided sample. The homogeneous dispersion of hydride in the sample implies that, even at this relatively initial stage of the hydriding reaction, most of the sample is already in the β form. This strongly suggests that hydrogen penetrating the sample through grain boundaries is spreading inside the grains in the form of β phase at relatively low concentrations. Then the reaction continues by dissolution of additional hydrogen in the β phase and subsequent $\beta \rightarrow \delta$ and $\delta \rightarrow \epsilon$ transformations.

3. The hydriding kinetics

In Fig. 4, the hydriding kinetics of zirconium below the eutectoid temperature (Fig. 4(a) for 400 °C, and Fig. 4(b) for 500 °C) is compared with the hydriding kinetics just above it. The measurements were performed

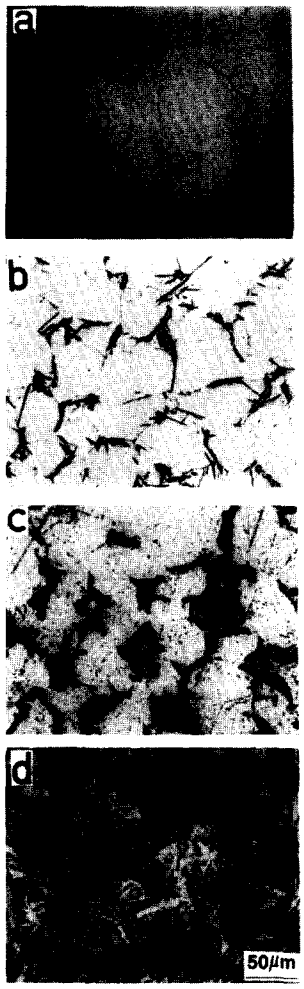

Fig. 3. The development of hydride phase in zirconium at 630 °C and under H_2 at 1 atm: (a) unreacted sample (pre-heated to 900 °C in vacuum like the partially reacted other samples); (b) the center part of partially reacted ($\alpha=0.023$) sample; (c) same as (b), but taken near the surface of the sample; (d) partially reacted ($\alpha=0.3$) sample.

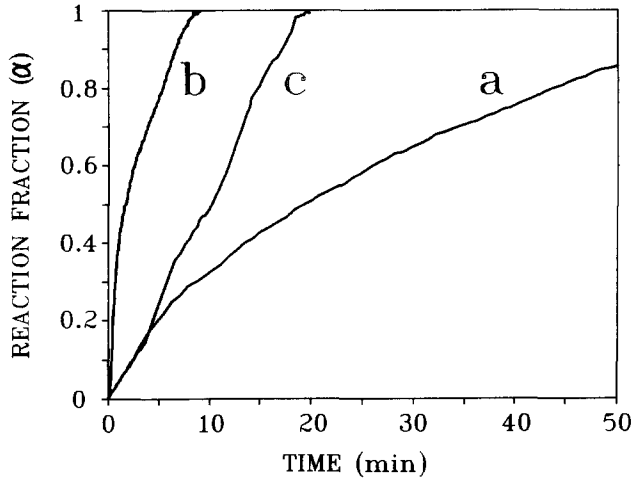

Fig. 4. The effect of temperature on the zirconium hydriding kinetics at the β phase formation threshold: curve a, 400 °C; curve b, 500 °C; curve c, 550 °C. All the samples have about the same geometry (cubes of around 1.8 mm length). The hydrogen pressure is 1 atm.

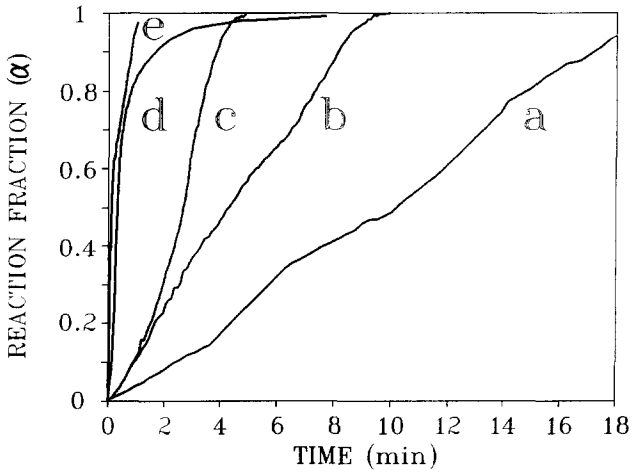

Fig. 5. The temperature dependence of the zirconium hydriding kinetics above the eutectoid temperature: curve a, 550 °C; curve b, 600 °C; curve c, 650 °C; curve d, 700 °C; curve e, 800 °C. The pressure and shape are the same as in Fig. 4.

on samples of similar shape and weight (cubes roughly 1.8 mm in length and of 30–40 mg mass) under hydrogen at 1 atm, to eliminate geometrical and pressure effects. At 400 °C the kinetic curve consists of two parts, as discussed above and in [1]. Raising the temperature to 500 °C results in an acceleration of both parts. It also changes the relative contributions of the two parts to the kinetics. The initial fast stage extends to higher α than at 400 °C. Since both the hydrogen solubility and the diffusion rate are higher at elevated temperatures, it is obvious that more hydrogen is able to penetrate through grain boundaries and to dissolve in the bulk during the initial stage. Thus the second stage is delayed at higher temperatures. This can also account for the excessive increase in hydriding rate at 500 °C, beyond that predicted by the Arrhenius law, as found by Une [5].

At 550 °C, however, the tendency is reversed. The hydriding rate is clearly slower than at 500 °C. Since up to the eutectoid temperature there is a continual increase in the hydriding reaction rate, this change should be attributed to the β phase formation (no measurements of the hydriding rates were performed below 400 °C since this range has been extensively studied in the past [5], and our results at 400 °C were in very good agreement with those previously obtained [1]). According to the metallographic examinations (Section 2), this decrease in the hydriding rate is associated also with the topochemical change, i.e. that grain boundary penetration becomes the dominant hydriding path.

Fig. 5 shows the temperature dependence of the hydriding kinetics between 550 and 800 °C. It is obvious that at this range the hydriding rate again increases with increasing temperature. In Fig. 6, a better time resolution of the higher temperature kinetics is presented by choosing a different (shorter) time scale. It

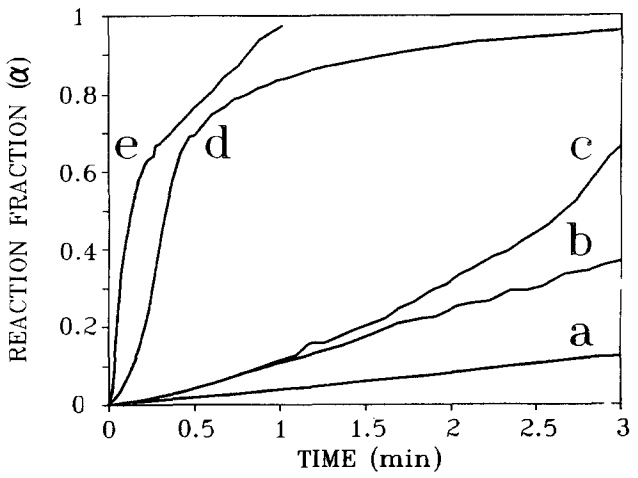

Fig. 6. An extension of Fig. 5 for the first 3 min, showing the high temperature hydriding kinetics with a better time resolution.

suggests that, besides the change in hydriding kinetics at the eutectoid temperature, above 550 °C the hydriding mechanism holds permanently for the whole high temperature range.

4. The change in hydriding mechanism below and above the eutectoid temperature

Before going on to a quantitative analysis of the results, the main differences between the hydriding mechanisms below and above the eutectoid temperature should be summarized. Let us designate the reaction mechanism above the eutectoid temperature as case A and that below the eutectoid temperature as case B. There are two observations indicating the change in mechanism.

(1) The hydriding reaction of the most general case B consists of two stages: initial grain boundary penetration followed by an external hydride layer formation. At temperatures below about 350 °C, the initial grain boundary attack cannot be observed (Fig. 1(a)). In case A, on the contrary, only the grain boundary path prevails.

(2) The overall hydriding rate in case A is lower than in case B, under similar conditions of pressure and temperature.

In the following, case B will be restricted to the high temperature range (above 350 °C) in which it consists of two detectable stages. To account for the differences between the two cases A and B, it should be remembered that initially both reaction rates are controlled by hydrogen flow through grain boundaries. This process is followed by the formation of a hydride layer at the grain circumference, advancing towards the grain centers. In case A, this layer consists of β phase, whereas in case B it is constructed mostly of the δ phase. The main difference between the two phases relevant to the hydriding mechanism is the different relative volume expansion associated with each of these transformations. The lattice parameters of the h.c.p. structure of the hydrogen-saturated α-Zr are $a_0 = 3.2335$ Å and $c_0 = 5.1520$ Å [12] (it should be mentioned that the increase in the lattice parameters per atomic per cent of hydrogen interstitial is much less than for both oxygen and nitrogen). The theoretical density of this structure is 6.49 g cm^{-3}. The hydrogen-induced β phase is a b.c.c. A2 structure type with $a_0 = 3.65$ Å for 20% overall hydrogen content, and 3.68 Å for 45% overall hydrogen content at 600 °C [13]. These values yield densities of 6.24 g cm^{-3} and 6.26 g cm^{-3} respectively. The δ-hydride is an f.c.c. (fluorite-type) structure with a lattice parameter ranging between 4.7789 Å for the low hydrogen content phase [14] and 4.7809 Å for the high hydrogen content phase (coexisting with the ϵ phase) [15]. On the assumption that 80% of the sites available for hydrogen are occupied, these values yield 5.65 g cm^{-3} and 5.64 g cm^{-3} respectively. Thus the formation of the δ-hydride is associated with volume expansion of 13.1%, whereas the formation of the β phase results in an expansion of 3.4% only. It is suggested that the larger volume expansion is responsible for the termination of the grain boundary penetration and the appearance of an external hydride layer in case B. The large volume expansion causes the reacting grains to be pressed together. This applied pressure gradually narrows the channel of transfer, reducing the hydrogen flow into the deeper parts of the sample. Eventually, the amount of hydrogen diffusing through the hydride layer become comparable with the flow through the grain boundaries. This is the turning point for the two stages. In case A, on the contrary, the volume expansion is not sufficiently large to reduce the transfer of hydrogen through the grain boundaries. Thus no external hydride layer is formed in case A.

5. Derivation of the front velocity in the grain boundary type of attack

5.1. Case A

In case A, the reaction can be assumed to advance simultaneously into each separate grain. This case is similar to that of a powder sample. In this work, the front velocity inside each grain is calculated from the experimental results using a simplified approximate approach. A more accurate derivation developed for the powder sample's case will be published separately [16].

On the assumption that the grains are spheres of radius r, it can be shown that a product front, starting its advance at all spheres simultaneously, moving inward at a constant velocity u yields

$$\alpha(t)=3\frac{ut}{r}-3\left(\frac{ut}{r}\right)^2+\left(\frac{ut}{r}\right)^3 \quad (1)$$

This equation is often presented in the contracting-volume form [17]:

$$1-(1-\alpha)^{1/3}=kt \quad (2)$$

where k is a rate constant (equal to u/r in Eq. (1)). It should be noted that tu is assumed to be constant. Of course, this assumption is not generally valid. However, it has been shown to apply to zirconium in case B [1,5]. Also, the initial stages of advance of any front, to which the following treatment is restricted, are usually obeying a linear kinetic behavior.

For the initial reaction stage, where the condition $ut \ll r$ is valid, Eq. (1) is approximately given by

$$\alpha \approx 3\frac{ut}{r} \quad (3)$$

Defining the initial slope $d\alpha/dt$ as the rate constant k_0, the initial front velocity into the grains can be obtained:

$$u=\tfrac{1}{3}k_0 r \quad (4)$$

The average grain size was estimated from metallographic examinations (see for example Fig. 1) to be about 25 μm. Thus, in case A, the front velocity of the grain boundaries can be calculated from the apparent initial rate constant k_0 and the average grain size. It should be emphasized that u is independent of the sample dimensions. It is related solely to the grain size.

5.2. Case B

This case is a little more complicated than the previous case. Initially, the grain boundary attack is very similar to that of case A. However, once an external hydride layer is formed, the grain boundary attack stops. At the time at which the external reaction front first appears, a layer of thickness l_{GB} has already been reacted through a grain boundary type of attack. Since the flux of hydrogen through the grain boundaries seems to be diffusion controlled, the quantity l_{GB} should be considered but as an effective thickness. Also, the change from grain boundary attack to external layer formation is expected to be gradual. Thus the determination of l_{GB} is rather a rough approximation. Still, as we shall see, quantitative information can be obtained even from such a rough evaluation.

For a parallelepiped sample of dimensions $a \times b \times c$, the volume of metal transformed until the first appearance of the external hydride layer is

$$V_{GB}=abc-(a-l_{GB})(b-l_{GB})(c-l_{GB})$$
$$=(ab+ac+bc)l_{GB}-(a+b+c){l_{GB}}^2+{l_{GB}}^3 \quad (5)$$

For $l_{GB} \ll a, b, c$, Eq. (5) can be given approximately by

$$V_{GB} \approx (ab+ac+bc)l_{GB} \quad (6)$$

The reaction fraction α_{GB} of this stage is defined as

$$\alpha_{GB}(t)=\frac{V(t)}{V_{GB}} \quad (7)$$

where $V(t)$ is the effective volume reacted until the time t. It should be noted that $\alpha_{GB}(t)$ is different from the overall reaction fraction $\alpha(t)$ defined as

$$\alpha(t)=\frac{V(t)}{V_0} \quad (8)$$

where V_0 is the initial volume of the sample (equal to abc, in this case).

Until the first appearance of the external hydride layer the situation is in fact identical with case A. Thus $\alpha_{GB}(t)$ can be given by Eq. (3).

From Eqs. (6)–(8), the relation between the measured $\alpha(t)$ and the system parameters can be obtained:

$$\alpha(t)=3l_{GB}\left(\frac{1}{a}+\frac{1}{b}+\frac{1}{c}\right)\frac{u_{GB}}{r}t \qquad \text{for } V(t)<V_{GB} \quad (9)$$

The velocity u_{GB} was indexed in Eq. (9) to distinguish it from the external layer velocity u. When the external layer first appears, the value of α_{GB} is equal to 1 and the overall reaction fraction α_l is given by

$$\alpha_l=\frac{V_{GB}}{V_0}=l_{GB}\left(\frac{1}{a}+\frac{1}{b}+\frac{1}{c}\right) \quad (10)$$

The initial reaction linear rate constant k_{GB} of this stage defined as $d\alpha/dt$ is given by

$$k_{GB}=3l_{GB}\left(\frac{1}{a}+\frac{1}{b}+\frac{1}{c}\right)\frac{u_{GB}}{r} \quad (11)$$

It is note worthy that k_{GB} is proportional to the sum of the reciprocals of the sample dimensions. In fact, such dependence has been proved for Zr at 400 °C by measuring the initial slopes of α vs. t kinetic curves for different planar samples of various initial thicknesses (see Fig. 6 in [1]). It has been shown, in addition, that the depth of the layer attacked in the grain boundaries below the external hydride front is about one grain size. That is, $l_{GB} \approx 2r$. Using this, and the value of $k_{GB}/(1/a+1/b+1/c)=134$ μm min^{-1} obtained from the slope of Fig. 6 in [1], the grain boundary velocity u_{GB} at the initial stage of zirconium hydriding at 400 °C is estimated as 22 μm min^{-1}. This value is, of course, different from the apparent (overall) initial velocity of 70 μm min^{-1} previously reported. It is still significantly higher, however, than the external hydride front velocity of 8 μm min^{-1} [1]. The reason for this difference will be accounted for in the next section.

The analysis of the kinetics at 500 °C is shown in Fig. 7. The two stages of the reaction are shown as lines a and b. There is a wide intermediate range between them which is the result of the gradual change from the grain boundary to the external layer mechanism, mentioned above. Despite this intermediate range, the two stages can be easily identified. The apparent linear rate constants for stages a and b are 0.8 min^{-1} and 0.07 min^{-1} respectively.

Using Eqs. (10) and (11), the value of u_{GB} can be evaluated:

$$u_{GB} = \frac{k_{GB} r}{3\alpha_l} \tag{12}$$

The value of α_l is roughly estimated from Fig. 7 as 0.13 ± 0.05. Thus the value of $u_{GB}(500\ °C) = 50\ \mu m\ min^{-1}$ is obtained.

The external hydride front velocity at 500 °C is calculated from the second rate constant (the slope in Fig. 7(b)) using the contracting-envelope procedure [1] to yield $u(500\ °C) = 25\ \mu m\ min^{-1}$.

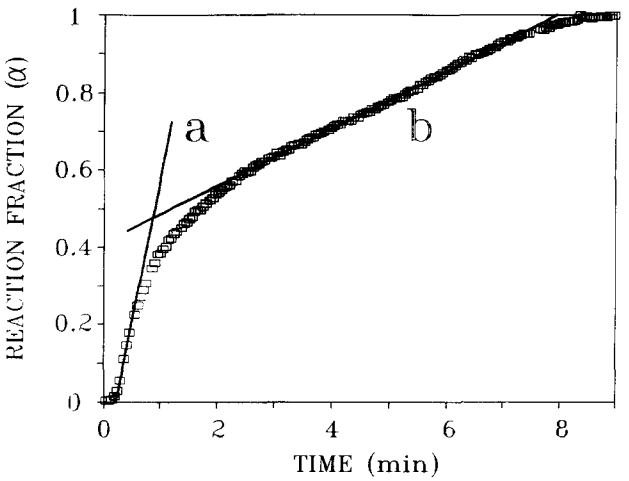

Fig. 7. The two stages in the hydriding kinetics of a parallelepiped Zr sample (dimensions, 2.1 mm×2.0 mm×1.56 mm) under H_2 at 1 atm and 500 °C: line a, initial grain boundary attack; line b, the second contracting envelope stage. The straight lines are the best-fitted slopes for the two stages.

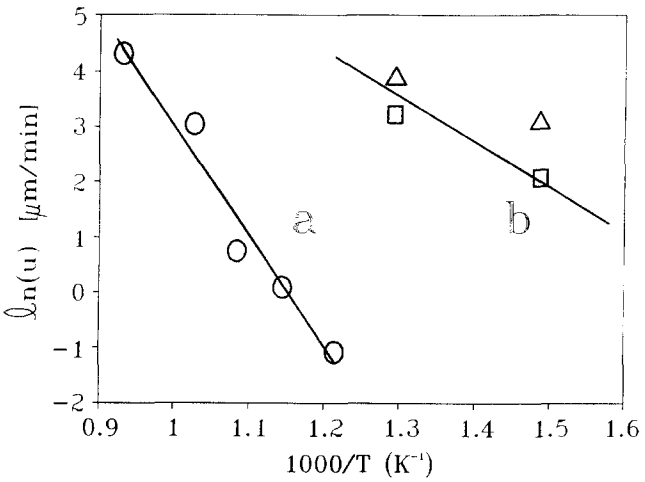

Fig. 8. The temperature dependence of the various hydride front velocities in the zirconium–hydrogen system under H_2 at 1 atm: line a, best linear regression fit above the eutectoid temperature; ○, experimental results for the grain boundary front velocity u_{GB} above the eutectoid temperature; line b, reaction rate constant below the eutectoid temperature reproduced from [5]; △, experimentally obtained values of u_{GB} below the eutectoid temperature; □, values of u below the eutectoid temperature.

6. The temperature dependence of the hydride front velocity in zirconium at high temperatures

The temperature dependence of the grain boundary velocity above the eutectoid temperature, calculated from Eq. (4) in Section 5.1, is shown in Fig. 8, line a. Below the eutectoid temperature, the values of u_{GB} and u, calculated in Section 5.2 for 400 and 500 °C, are shown in Fig. 8b. For comparison, the best-fitted Arrhenius plot obtained for Zircaloy-2 in the temperature range 300–450 °C [5], is also shown by the straight line b in Fig. 8. Our experimental results are in good agreement with this plot. The grain boundary front velocity u_{GB} is faster than the external layer front velocity u (see Section 5.2). The activation energies for the two velocities are comparable, however, suggesting that both are controlled by the same step (i.e. diffusion through the constant-thickness product layer). The speed difference may be correlated with the effective steady state thicknesses of the hydride layers of the two topochemical processes. The layer formed along the grains circumferences is probably thinner than that formed subsequently over the sample surface. Since both layer advances are diffusion controlled, the velocity of the thinner layer should be faster.

The temperature dependence of the grain boundary front velocity u_{GB} above the eutectoid temperature is indicative of a complete change in the reaction mechanism. Not only is the magnitude of the velocity decreased by a factor of about 150 between 500 and 550 °C, but also the best-fitted activation energy is 165 kJ mol^{-1}, compared with the value of 68.2 kJ mol^{-1}, obtained for the front velocity below the eutectoid temperature [5] (from line b in Fig. 8). The change in mechanism is obviously associated with the appearance of the β phase intermediate layer above 550 °C. We have mentioned earlier that this appearance can lead to a change in the steady state thickness of the δ hydride layer, thus resulting in a discontinuous change in the temperature dependence of the front velocity, while keeping the activation energy unchanged. The results shown in Fig. 8, however, indicate than the activation energy is actually changing. This means

that the rate-limiting step has been changed. The grain boundary topochemistry observed in this case eliminates a surface-controlled rate limiting step. Thus there are two other possible rate-determining steps left: diffusion through the β phase, and the $\alpha \rightarrow \beta$ phase transformation. These two possibilities will be discussed in the next section.

7. The hydriding rate-limiting step above the eutectoid temperature

As mentioned above (Section 1), large discrepancies were found in measuring the activation energy for hydrogen diffusion through the β phase zirconium. Thus, the values reported were 192 kJ mol^{-1} by Albrecht and Goode [7], 35.7 kJ mol^{-1} by Someno [18] and 34.8 kJ mol^{-1} by Gelezunas et al. [6]. The activation energy in the present case (165 kJ mol^{-1}) is comparable with the higher of these values. It is even in better agreement with the value of 146 kJ mol^{-1}, measured for hydrogen permeation in zirconium containing 60–65 at.% H, in the temperature range 500–750 °C by Albrecht and Goode [19]. Since in their experiment the zirconium was allowed to reach equilibrium in the hydride phase, the diffusion was assumed to take place in a higher hydride (possibly the δ and $\delta+\epsilon$ regions [3]). However, this value was much higher than the average activation energy of 67 ± 17 kJ mol^{-1} found for these regions by several independent workers, which was also in good agreement with the kinetic results (see [20] and discussion in [1]). To account for this discrepancy, suppose the sample in the permeation experiment [18] has not been entirely transformed into the δ and $\delta+\epsilon$ phases. In the depth of the sample (it was 1–1.5 mm thick [18]) some residual β phase layer still exists. It should be remembered that the eutectoid reaction and the $\alpha \rightarrow \beta$ phase transformation are considered to be extremely sluggish [3]. This residual β phase layer could account for the high activation energy obtained in the permeation experiments as well as for good agreement with the present activation energy. It also explains the similarity of the activation energies measured by these workers for the low concentration (β phase) region, and for the high concentration (δ and $\delta+\epsilon$ phases) region, (i.e. 192 kJ mol^{-1} [7] and 146 kJ mol^{-1} [19] respectively).

The significantly higher diffusion coefficients obtained by Gelezunas et al. [6] require some consideration. The experimental set-up in their work was based on an accurate gas absorption measurement system. The zirconium samples were machined into cylinders and spheres of about 7 mm radii. These samples were heated in vacuo at 960 °C prior to the experiment. This procedure is very similar to the heat pre-treatment in the present work, which has been shown to induce a grain boundary type of hydridization. This possibility was not taken into account by Gelezunas, who assumed that diffusion occurred over the whole spherical sample. The validity of the diffusion-controlled rate-limiting step in his case has been tested by comparing the experimental sorption results with the diffusion theoretical curves. However, as implied in the present work, this test will be satisfactory also for grain boundary penetration. The only difference between the two cases is the diffusion distance given by the sample radius (as assumed by Gelezunas et al.) in contrast with the grain size (as in the present work). This could account for the difference in the absolute values of the diffusion coefficients (by a factor equal to the square of the ratio of these sizes), but not for the difference in the activation energies. However, in the relatively large samples used in that work, grain boundary diffusion may have an additional effect.

The two representative cases discussed above demonstrate once again the importance of combining metallographic examinations of partially reacted samples in the study of metal hydriding kinetics.

There is almost no published information on the kinetics of the $\alpha \rightarrow \beta$ phase transformation in the presence of hydrogen. As mentioned above, the eutectoid reaction (i.e. the $\alpha+\delta \rightarrow \beta$ reaction) is extremely sluggish on heating [12]. The $\alpha \rightarrow \beta$ transformation is expected to be somewhat faster, because less hydrogen redistribution is required in the later case [3]. In order to distinguish between the two possible rate-limiting steps, namely diffusion and transformation, more data is needed concerning the pressure dependence of the hydride front velocity, the effect of grain size etc.

8. Conclusions

The mechanism of the hydriding reaction of vacuum-annealed zirconium is temperature dependent regarding both the topochemistry and the rate-determining step.

Below about 350 °C, the product hydride layer is formed on the sample surface, moving into the sample in a contracting-envelope type of attack. The reaction front velocity is constant. The rate-determining step is diffusion through a hydride (most probably the δ phase) layer of constant steady state thickness (the layer is built into the sample and cracked at its external side).

Between 350 and 550 °C, the reaction consists of two stages: initial grain boundary penetration followed by external layer formation. The initial stage is terminated as the expanding δ-hydride presses the grains together, preventing further hydrogen flux through this path. The rate-determining step in both stages is the

same as above (i.e. diffusion controlled). The front velocity at the grain circumference is higher than the external layer velocity, probably owing to different steady state layer thicknesses.

The activation energy for the hydriding is equal to that of the diffusion of hydrogen through the δ-hydride, i.e. around 67 kJ mol^{-1}.

Above 550 °C, the eutectoid temperature, the topochemistry and the rate-determining step change. Grain boundary attack prevails throughout the reaction. No external layer is observed. The reason for the change in topochemical attack is the smaller expansion of the β phase, relative to that of the δ-hydride, which does not prevent hydrogen flux through the grain boundaries.

The rate-determining step is either diffusion through the β phase or the $\alpha \rightarrow \beta$ phase transformation. The activation energy for the front velocity is about 165 kJ mol^{-1}. This value is comparable with some published data of hydrogen diffusion in the β phase.

Acknowledgments

The technical assistance of Mr. Ari Kremner is gratefully acknowledged. Thanks are also due to Y. Zeiri, I. Jacob and M.H. Mintz for helpful discussions. This research was partially supported by a joint grant from the Israel Council for Higher Education and Israel Atomic Energy Commission.

References

[1] J. Bloch, I. Jacob and M.H. Mintz, *J. Alloys Comp., 191* (1993) 179.
[2] J. Belle, B.B. Cleland and M.W. Mallett, *J. Electrochem. Soc., 101* (1954) 211.
[3] W.M. Mueller, J.P. Blackledge and G.G. Libowitz, *Metal Hydrides,* Academic Press, New York, 1968, Chapter 7.
[4] G. Kuus and W. Martens, *J. Less-Common Met., 75* (1980) 111.
[5] K. Une, *J. Less-Common Met., 57* (1978) 93.
[6] V. Gelezunas, P.K. Conn and R.H. Price, *J. Electrochem. Soc., 110* (1963) 799.
[7] W.M. Albrecht and W.D. Goode, *Rep. BMI-1373,* 1959 (Battelle Memorial Institute).
[8] P.E. West and P.M. George, *J. Vac. Sci. Technol. A, 5* (1987) 1124.
[9] E. Swissa, N. Shamir, M.H. Mintz and J. Bloch, *J. Nucl. Mater., 173* (1990) 87.
[10] J.J. Kearns, *J. Nucl. Mater., 22* (1967) 292.
[11] J. Bloch, Z. Hadari and M.H. Mintz, *J. Less-Common Met., 102* (1984) 311.
[12] R.L. Beck, *Am. Soc. Met. Trans. Q., 55* (1962) 542.
[13] D.A. Vaughan and J.R. Bridge, *J. Met., 8* (1956) 528.
[14] C.P. Kempter, R.O. Elliot and K.A. Geschneider, Jr., *J. Chem. Phys., 33* (1960) 837.
[15] W.L. Korst, *USAEC Rep. NAA-SR-6880,* 1962 (Atomics International) (US Atomic Energy Commission Contract).
[16] M.H. Mintz and Y. Zeiri, *J. Alloys Comp.,* in press.
[17] D.W. Johnson and P.K. Gallagher, *J. Phys. Chem., 75* (1971) 1179.
[18] M. Someno, *Nippon Kinzoku Gakkaishi, 24* (1960) 249.
[19] W.M. Albrecht and W.D. Goode, *Rep. BMI-1426,* 1960 (Battelle Memorial Institute).
[20] P. Paetz and K. Lücke, *Z. Metallkd., 62* (1971) 657.